

Phase diagram and tie-line determination for the ternary mixture DOPC/eggSM/Cholesterol

Supporting Material

N. Bezlyepkina, R. S. Gracià[†], P. Shchelokovskyy, R. Lipowsky and R. Dimova*

Max Planck Institute of Colloids and Interfaces, Science Park Golm, 14424 Potsdam, Germany

[†] Present address: Culgi B.V., P.O. Box 252, 2300 AG Leiden, The Netherlands

* Address correspondence to Rumiana.Dimova@mpikg.mpg.de

1. Phase diagram of the DOPC/SM/Chol mixture

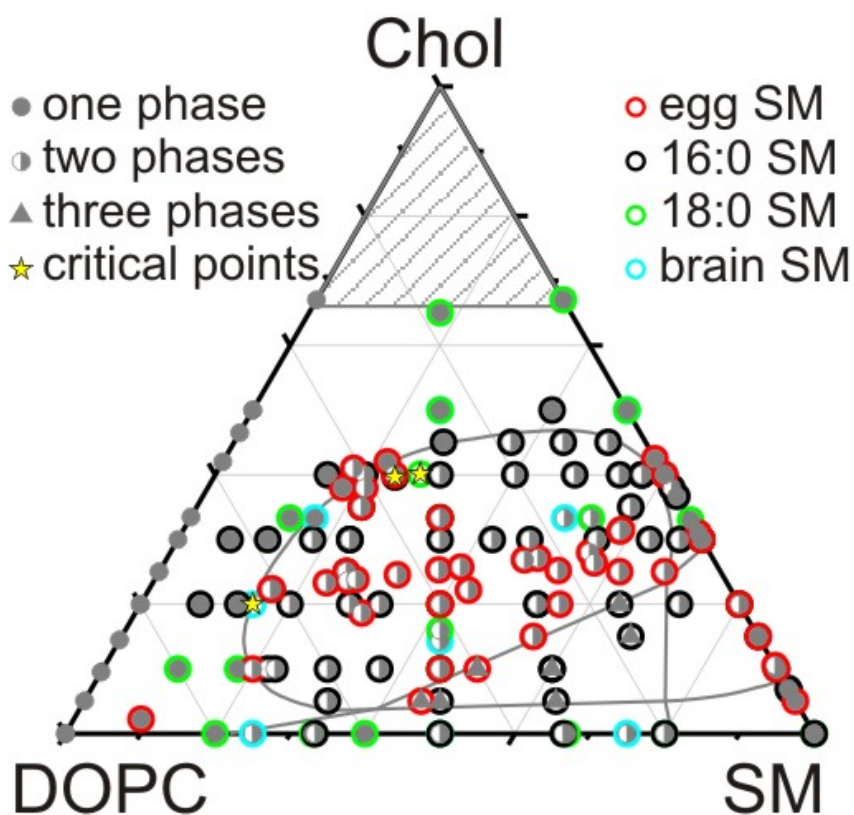


FIGURE S1 Phase diagram of the ternary mixture DOPC/SM/Chol at $(23\pm 1)^\circ\text{C}$. Data available in the literature (see main text for references) and our own data were grouped according to the number of observed coexisting phases (left legend) and SM type (right legend). Stars indicate reported critical points, see text for details. The figure represents a larger version of Fig. 1A in the main text.

2. Experimental chambers for vesicle electrofusion

Two observation chambers were used. One was purchased from Eppendorf (Hamburg, Germany) and modified as described below. The other was home-made and used for electrofusion assisted with micropipettes.

The original Eppendorf chamber consisted of a Teflon frame with a circular opening confined from below by a glass plate, see Fig. S2A. A pair of parallel platinum wires (92 μm in radius) with a gap distance of 500 μm was fixed to the glass. The thickness of the glass plate below the electrodes in the original chamber was larger than the working distance of the objectives used for recordings at the confocal microscope, which is why we removed the glass plate below the electrodes, see Fig. S2B. This has allowed the use of glass slides with the desired thickness. The vesicle solution was placed in the cavity of the observation chamber and closed with glass from above so that observation of the space between the electrodes was possible under the microscope in both fluorescence and transmission mode.

To create a suitable electrofusion chamber which allows for access of micropipettes, two Teflon frames of specially designed shape with fixed platinum electrode wires were used, see Fig. S2C. The platinum wires had a diameter of 0.2 mm or 0.5 mm. The Teflon frames were placed between two glass slides and fixed with silicon (CAF4, Rhone Poulenc, France). The space between the glass slides was about 5 mm. The chamber was open from two opposite sides to allow insertion of micropipettes.

The chamber was filled almost completely with glucose solution. The solutions of the different vesicle types were added afterwards from the different sides of the chamber. As such we had two vesicle reservoirs from which to select the vesicles with appropriate composition and size. The vesicles settled at the bottom of the observation chamber. A selected vesicle was weakly aspirated into a micropipette so that it was enough to hold and move it. Then, it was brought in close proximity to another aspirated vesicle in such a way that the axis connecting the centers of the external vesicle caps was perpendicular to the electrodes. Depending on the vesicle composition and size, the applied pressure could be varied to reach favorable electrofusion conditions.

The electrodes were connected by clips to the Multiporator to apply DC pulses. The distance between the electrodes was not constant for every chamber assembly since the electrodes were not parallel to each other but somewhat bent, see Fig. S2C, and this distance was adjusted by hand. To calculate the applied electric field, the distance between the electrodes was measured individually after each successful electrofusion event. When a given electric pulse has led to fusion, the pressure in one of the micropipettes was released so that the formed vesicle was held by one micropipette only.

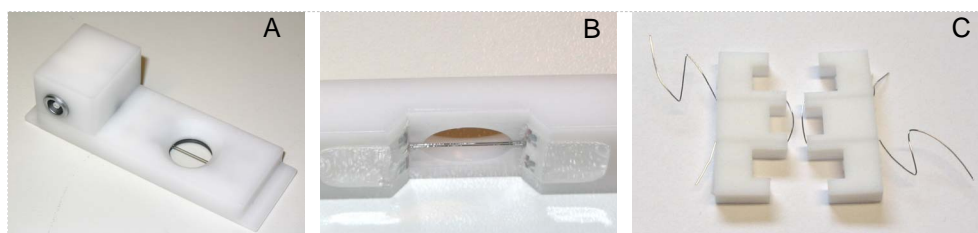


FIGURE S2 Electrofusion chambers. (A) Original Eppendorf chamber (top view); (B) Chamber modified for experiments at the confocal microscope (view from below); (C) The home-made chamber (without the covering glass slides) used for electrofusion with micropipette assistance.

3. Aberration corrections in the image analysis

By default, the home-made software for image analysis reconstructs the vesicle shape assuming the voxel to be cubic, i.e. taking the distance between the contours in the different slices to be the same as the pixel size, which is usually not true in confocal microscopy. In addition, spherical aberration may be introduced due to refractive index mismatch between the immersion medium and the specimen, deforming an image along the z -axis in three dimensional stack acquisitions. These aberrations can be corrected in the first approximation by simple rescaling of the z -axis in the data with the ratio of the refractive indices (1). To validate this approximation for our system Fluoresbrite YG 20.0 micron microspheres (Polysciences Inc., excitation 441 nm, emission 486 nm, $d = 18.6 \pm 2.53 \mu\text{m}$) were used to measure the particle size distortion along the z -axis in different media and with different objectives. The image of a particle in the xz plane (vertical cross section) was recorded with the confocal microscope. The particle diameters d_x and d_z as measured along the x - and the z -axis were found. Their ratio, d_x/d_z , was compared with the ratio of the refractive indices of the sample medium, n_s , and of the immersion medium, n_{imm} . Results of these measurements confirmed that those ratios are in close agreement, within a relative error of 8%. Thus, the correction factor Z_{corr} used for the z -axis rescaling of the vesicle images in the home-made software was calculated as the product of the ratio a_z/a_x between the axial and the lateral voxel sizes, a_z and a_x , respectively, (these were taken from the Leica microscope control software) and of ratio of the sample and immersion media refractive indices, $Z_{corr} = (a_z/a_x) \times (n_s/n_{imm})$.

4. Calculating the precise composition of a vesicle obtained by electrofusion

To determine the vesicle composition from the domain areas, we used the following procedure. From the first confocal series recorded right after the electrofusion event, we measured the surface areas of the green (l_o phase) and the red (l_d phase) domains, S_{green} and S_{red} , respectively. Since lipid redistribution usually takes longer than tens of minutes, we assumed that the composition of each domain in this first confocal series is identical to the corresponding compositions of the initial vesicles before fusion. For the green domain, we denote the mole fractions of SM and Chol with $f_{SM,initial}$ and $f_{Ch,initial}^{l_o}$ respectively. For the red domain, we denote the mole fractions of DOPC and Chol with $f_{DOPC,initial}$ and $f_{Ch,initial}^{l_d}$, respectively. From literature data on the areas per molecule for SM, Chol and DOPC, the area of the domains and their initial composition, we can calculate the exact composition of the fused vesicle as explained further below.

We denote the molecular surface area of each lipid in the different phases as $A_{SM}^{l_o}$ for eSM in the l_o phase, $A_{DOPC}^{l_d}$ for DOPC in the l_d phase, and $A_{Ch}^{l_o}$ and $A_{Ch}^{l_d}$ for Chol in the l_o and the l_d phase, respectively. We calculate the respective number of molecules, N_{SM} , N_{DOPC} , and N_{Ch} , in the vesicle produced by electrofusion as follows:

$$\begin{aligned}
N_{SM} &= \frac{S_{green}}{A_{SM}^{lo} + \frac{f_{Ch,initial}^{lo}}{f_{SM,initial}} A_{Ch}^{lo}}, & N_{DOPC} &= \frac{S_{red}}{A_{DOPC}^{ld} + \frac{f_{Ch,initial}^{ld}}{f_{DOPC,initial}} A_{Ch}^{ld}}, \\
N_{Ch} &= \frac{S_{green}}{A_{Ch}^{lo} + \frac{f_{SM,initial}^{lo}}{f_{Ch,initial}} A_{SM}^{lo}} + \frac{S_{red}}{A_{Ch}^{ld} + \frac{f_{DOPC,initial}^{ld}}{f_{Ch,initial}} A_{DOPC}^{ld}}.
\end{aligned} \tag{1}$$

The total number of molecules is:

$$N = N_{SM} + N_{Ch} + N_{DOPC}. \tag{2}$$

Finally, the lipid mole fractions in the final vesicle, f_{SM} , f_{DOPC} , and f_{Ch} , i.e., the vesicle composition, will be:

$$f_{SM} = \frac{N_{SM}}{N} \times 100\%, \quad f_{DOPC} = \frac{N_{DOPC}}{N} \times 100\% \quad \text{and} \quad f_{Ch} = \frac{N_{Ch}}{N} \times 100\%. \tag{3}$$

There are three possible sources of errors in the calculation of the vesicle composition: error in measuring the surface areas of the domains in the fused vesicle (S_{green} and S_{red}), uncertainty of the area per molecule of the different lipids in the initial vesicles (A_{SM}^{lo} , A_{DOPC}^{ld} , A_{Ch}^{lo} and A_{Ch}^{ld}) and error due to imperfect compositions of these vesicles (i.e., error in $f_{SM,initial}$, $f_{Ch,initial}^{lo}$, $f_{DOPC,initial}$ and $f_{Ch,initial}^{ld}$). We neglect the latter error source, since the vesicles were prepared and stored at temperature at which the lipid components were fully miscible. We are then left with two error sources that we consider to be independent: the error stemming from the image processing procedure to extract the domain areas and the uncertainty of areas per lipid molecule.

Image processing: The vesicles are digitized by manual processing of confocal stacks. Thus, the main source of error comes from manually assigning contours to vesicle slices, since the software gives only approximate guides to help the human processing. In order to estimate the associated error, two authors of this study independently digitized 9 vesicles to measure domain areas and these sets of values were used to calculate the lipid composition (for fixed areas per lipid molecules). The maximal standard deviation was then calculated to be 2% of the mean for the domain area fractions and for the lipid composition 2.0 mol% for DOPC, 1.8 mol% for SM and 0.3 mol% for Chol as obtained from analytical estimates for error propagation. We take the largest of these three (2.0 mol% for DOPC) as the estimate of the error due to manual image processing and vesicle digitalization.

Areas per lipid molecule: There are no systematic data about how the areas per lipid change with membrane composition. Thus, we used values interpolated to our conditions from the data available in the literature (2-7): 51 Å² for SM (3), 27 Å² for cholesterol (3, 4), 70 or 66 Å² for DOPC with 10 or 20 mol% of Chol (5, 6), respectively. We varied the area per molecule in the ranges 46 – 53 Å² for SM, 25 – 31 Å² for Chol, 70 – 72 Å² for DOPC when mixed with 10 mol % Chol, and 66 – 68 Å² for DOPC when mixed with 20 mol % of Chol. To evaluate the error in the vesicle composition associated with the uncertainty in the areas per lipid, we performed Monte-Carlo simulation of the error propagation. From each of the above-indicated ranges for the lipid area per molecule, we drew 1 million samples assuming uniform distribution and calculated the corresponding vesicle composition and the standard deviation for all 13 vesicles analyzed. The standard deviation of the vesicle composition associated with the uncertainty in the lipid area per molecule was found to be 0.6 mol% for DOPC, 0.5 mol% for SM and 0.1 mol% for Chol as averaged between the vesicles. We also tested other ranges for the areas per lipid. If we take the values of the area per lipid as indicated in the main

text (see also Table S1), and allow a deviation of $\pm 1 \text{ \AA}^2$ for all three lipids, by the procedure above we get 0.2 mol% average standard deviation, $\pm 2 \text{ \AA}^2$ deviation produces 0.4 mol% average standard deviation and $\pm 3 \text{ \AA}^2$ deviation results in 0.6 mol% average standard deviation.

Total error: We consider the two error contributions described above to be statistically independent. Then, the total standard deviation of the lipid composition can be estimated by taking the square root of the sum of the squared standard deviations of the contributing errors. Combining data from Monte-Carlo simulations of the error propagation for the area per lipid and analytical results for the error propagation for the image processing we estimate the standard deviations in the composition to be 2.1 mol% for DOPC, 1.9 mol% for SM and 0.3 mol% for Chol. We have also performed the Monte-Carlo simulation with all parameters randomized – with the lipid areas uniformly distributed, as described above, and with the domain areas normally distributed with mean value and standard deviation as estimated by our two-user analysis. This approach produced estimation of the total standard deviation of the composition to be 2.1 mol% for DOPC, 1.7 mol% for SM and 0.3 mol% for Chol. As these two ways of the error estimate produce similar results, we use the largest of these values (2.1 mol% for DOPC) as a general estimation of the accuracy of our method with respect to the lipid composition of the final vesicle.

5. Compositional inhomogeneity of vesicles prepared from ternary lipid mixtures

Figure S3 illustrates the compositional inhomogeneity of vesicles prepared from a ternary lipid mixture located close to the boundary of the l_o - l_d coexistence region.

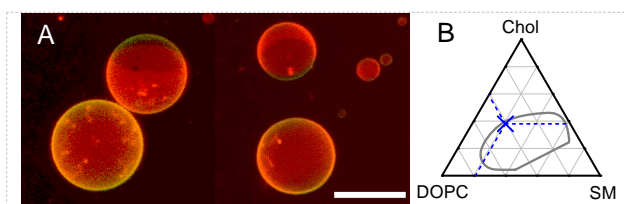


FIGURE S3 Compositional inhomogeneity of vesicles prepared from DOPC/eSM/Chol (41/21/38) mixture. (A) Two snapshots of 3D projections made from confocal series. Vesicles with domains (upper parts of the images) and vesicles without domains (lower parts of the images) coexist in the same sample. The scale bar is 50 μm . (B) Lipid composition (blue cross) in the Gibbs triangle. The grey curve shows the boundary of the l_o - l_d coexistence region.

6. Tie-line search procedure

The boundary of the region of l_o - l_d coexistence was represented as a polygon of 70 connected points. The proposed tie-line determination method consists of the following steps.

Step 1: Draw a line through the point corresponding to the vesicle composition on the phase diagram – we term this tie line “a hypothetical tie line” (Fig. S4). Read the coordinates at the intersections of the hypothetical tie line with the l_o - l_d region boundary. These coordinates yield the

compositions of the liquid ordered $\{f_{DOPC}^{l_o}, f_{SM}^{l_o}, f_{Ch}^{l_o}\}$ and the liquid disordered $\{f_{DOPC}^{l_d}, f_{SM}^{l_d}, f_{Ch}^{l_d}\}$ phases, where $f_{DOPC}^{l_i}, f_{SM}^{l_i}$ and $f_{Ch}^{l_i}$ are the mole fractions of the respective molecules in the corresponding phase (here l_i indicates either the l_o or the l_d phase).

Step 2: Calculate the surface areas of the phases according to the hypothetical tie line, $S_{tie\ line}^{l_o}$ and $S_{tie\ line}^{l_d}$, as sums of the surface areas occupied by all molecules in the corresponding phase:

$$S_{tie\ line}^{l_o} = N_{SM}^{l_o} A_{SM}^{l_o} + N_{Ch}^{l_o} A_{Ch}^{l_o} + N_{DOPC}^{l_o} A_{DOPC}^{l_o} \quad (4a)$$

$$S_{tie\ line}^{l_d} = N_{SM}^{l_d} A_{SM}^{l_d} + N_{Ch}^{l_d} A_{Ch}^{l_d} + N_{DOPC}^{l_d} A_{DOPC}^{l_d} \quad (4b)$$

where $A_{SM}^{l_o}, A_{Ch}^{l_o}, A_{DOPC}^{l_o}$ and $A_{SM}^{l_d}, A_{Ch}^{l_d}, A_{DOPC}^{l_d}$ are the corresponding molecular surface areas of the lipids in the l_o or l_d phase; $N_{SM}^{l_o}, N_{Ch}^{l_o}, N_{DOPC}^{l_o}$ and $N_{SM}^{l_d}, N_{Ch}^{l_d}, N_{DOPC}^{l_d}$ are the numbers of molecules in the l_o or l_d phase that can be calculated as follows.

The areas per molecule for the lipids in the different phases are given in Table S1. For the molecular area of DOPC in Eq. (4a-b), we have assumed a linear dependence on the cholesterol content and have taken interpolated values from data in the literature.

Table S1 Molecular surface areas of the different lipids used for the calculations of surface areas of the phases according to the hypothetical tie lines. The values correspond to room temperature.

Lipid	Area, Å ²	References
DOPC	71	(5-7)
+ 10 mol% Chol	70	
+ 20 mol% Chol	66	
+ 30 mol% Chol	66	
+ 40 mol% Chol	63	
SM	45	(2, 3)
+ 30 mol% Chol	51	
Chol	27	(3, 4)

The fraction of SM molecules in the l_o or l_d phases is defined as the ratio of the SM molecules number to the number of all molecules, N^{l_o} or N^{l_d} , in the corresponding phase:

$$f_{SM}^{l_o} = \frac{N_{SM}^{l_o}}{N^{l_o}} \quad (5a)$$

$$f_{SM}^{l_d} = \frac{N_{SM}^{l_d}}{N^{l_d}} \quad (5b)$$

The total number of SM molecules in the vesicle is a sum of the number of SM molecules in the l_o and l_d phases or is a product of the total number of lipids and the fraction of SM molecules in the vesicle:

$$N_{SM} = N_{SM}^{l_o} + N_{SM}^{l_d} \equiv N f_{SM} \quad (6)$$

From Eqs. (5 – 6) the number of SM molecules in the l_o phase is:

$$N_{SM}^{l_o} = f_{SM}^{l_o} N^{l_o} \equiv N_{SM} - N_{SM}^{l_d} \quad (7a)$$

$$N_{SM} - N_{SM}^{l_d} = N_{SM} - f_{SM}^{l_d} (N - N^{l_o}) \quad (7b)$$

$$N^{lo} = \frac{N_{SM} - f_{SM}^{ld} N}{f_{SM}^{lo} - f_{SM}^{ld}} = N \frac{f_{SM} - f_{SM}^{ld}}{f_{SM}^{lo} - f_{SM}^{ld}} \quad (7c)$$

$$N_{SM}^{lo} = f_{SM}^{lo} N^{lo} = f_{SM}^{lo} N \frac{f_{SM} - f_{SM}^{ld}}{f_{SM}^{lo} - f_{SM}^{ld}} \quad (7d)$$

Then, the number of SM molecules in the l_d phase is

$$N_{SM}^{ld} = N_{SM} - N_{SM}^{lo} = N_{SM} - f_{SM}^{lo} N \frac{f_{SM} - f_{SM}^{ld}}{f_{SM}^{lo} - f_{SM}^{ld}} \quad (8)$$

The total number of molecules $\{N_{SM}, N_{Ch}, N_{DOPC}\}$ and the composition of the vesicle $\{f_{SM}, f_{Ch}, f_{DOPC}\}$ was calculated from the confocal images recorded right after the vesicle electrofusion as described in Section 4 of the Supporting Material.

The numbers of cholesterol and DOPC molecules in the corresponding phases are calculated in a similar fashion yielding:

$$N_{Ch}^{lo} = f_{Ch}^{lo} N \frac{f_{Ch} - f_{Ch}^{ld}}{f_{Ch}^{lo} - f_{Ch}^{ld}} \quad (9a)$$

$$N_{Ch}^{ld} = N_{Ch} - f_{Ch}^{lo} N \frac{f_{Ch} - f_{Ch}^{ld}}{f_{Ch}^{lo} - f_{Ch}^{ld}} \quad (9b)$$

$$N_{DOPC}^{lo} = f_{DOPC}^{lo} N \frac{f_{DOPC} - f_{DOPC}^{ld}}{f_{DOPC}^{lo} - f_{DOPC}^{ld}} \quad (10a)$$

$$N_{DOPC}^{ld} = N_{DOPC} - f_{DOPC}^{lo} N \frac{f_{DOPC} - f_{DOPC}^{ld}}{f_{DOPC}^{lo} - f_{DOPC}^{ld}} \quad (10b)$$

Step 3: From the areas of the phases estimated from the hypothetical tie line, $S_{tie\ line}^{lo}$ and $S_{tie\ line}^{ld}$, and those measured from the confocal image of the vesicle after equilibration, S_{eq}^{lo} and S_{eq}^{ld} , calculate the differences $\Delta\bar{s}$ between the hypothetical and measured domain area fractions for the liquid ordered or disordered phases:

$$\Delta\bar{s} = \left| \frac{S_{tie\ line}^{ld}}{S_{tie\ line}^{ld} + S_{tie\ line}^{lo}} - \frac{S_{eq}^{ld}}{S_{eq}^{ld} + S_{eq}^{lo}} \right| \equiv \left| \frac{S_{tie\ line}^{lo}}{S_{tie\ line}^{ld} + S_{tie\ line}^{lo}} - \frac{S_{eq}^{lo}}{S_{eq}^{ld} + S_{eq}^{lo}} \right|.$$

Step 4: Apply the selection criterion $\Delta\bar{s} < 2\%$, as set by the uncertainty in surface area measurements resulting from manual processing. If this selection criterion is fulfilled, i.e., the hypothetical tie line becomes a trial tie line, proceed to the following step. If not, draw another hypothetical tie line and repeat the procedure from Step 1.

Step 5: From all trial tie lines found for each measured vesicle composition, make a choice in such a way that:

- i) The boundary between the region of l_o - l_d coexisting phases and the region of s - l_o - l_d coexisting phases represents a tie line (called the end tie line).
- ii) Tie lines do not cross each other inside the l_o - l_d coexistence region.

The search procedure is illustrated in Fig. S4. The procedure was automated with the help of home-written software.

To draw the hypothetical tie lines in the l_o - l_d region of the phase diagram, a series of lines with 1 degree of arc increment in slope angle was plotted through the selected composition point. The corresponding hypothetical domain surface areas were calculated for each line. After applying the selection criteria in Step 4 and the rules in Step 5 in the search procedure, we obtain the coordinates of the trial tie lines. Examining all composition points of the equilibrated fused vesicles, no trial tie lines for 4 out of the 13 composition points were found for the defined coexistence curve.

We then allowed for some deviation from the defined coexisting curve and the procedure was repeated. Deviation from the coexistence curve was done with a step of 0.5 mol% both inward and outward along the trial direction. All possible combinations of inward and outward deviations for both hypothetical tie-line ends were tested for acceptance. Thus, several line segments on each line plotted through the composition point were taken to calculate the fraction surface areas. The number of line segments and their end coordinates were specified by the allowed boundary deviation. This implies that if, for example, the boundary deviation was set to be 2 mol% then each line contained 81 segments (9 possible coordinates for each side).

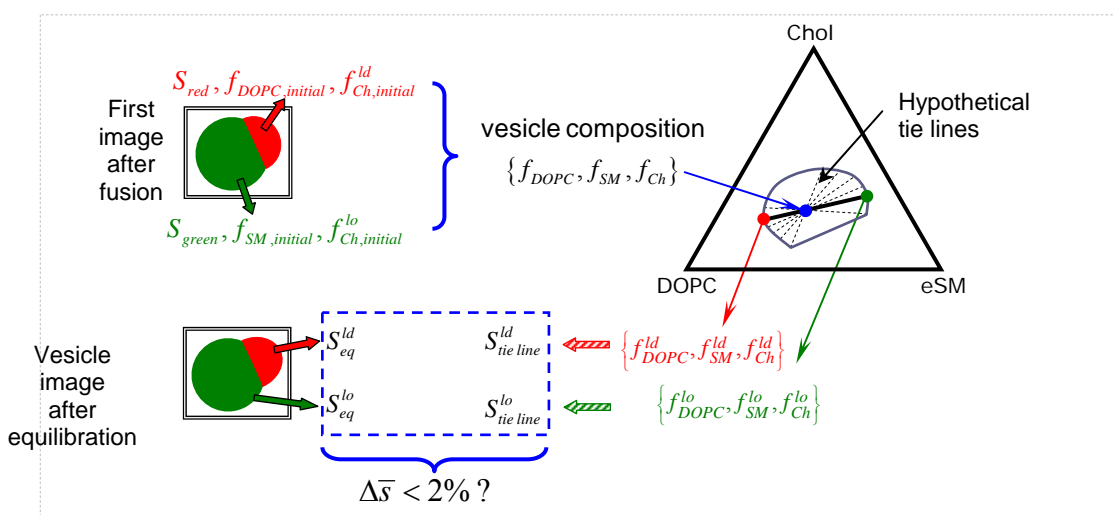


FIGURE S4 A schematic illustration of the procedure for searching for trial tie lines. From the first image collected right after fusion, we measure the areas of the domains. Knowing the domain composition and the area, we determine the total composition of the fused vesicle as marked by the blue circle in the phase diagram. Hypothetical tie lines are drawn through this compositional point. Their intersections with the boundary of the l_o - l_d coexistence region define the hypothetical compositions of the liquid phases in the equilibrated vesicle. From these compositions, the hypothetical areas of the equilibrated domains are calculated and compared to the areas of the domains measured in the image of the vesicle after equilibration following the selection criteria as explained in the text.

After allowing for boundary deviation, altogether 22857 trial tie-lines were found, yielding about 2×10^{22} possible sets of tie lines (intersecting and non-intersecting). Although the software was designed to search and select only non-intersecting lines, it would take too long to test and find this subset. To reduce the number of trial tie-lines, only one line segment for a given direction which gave minimal value of $\Delta \bar{s}$ was considered, if more than one segment on given line met the condition $\Delta \bar{s} < 2\%$. This condition reduced the number of trial tie lines down to 702. Manually this number was further reduced down to 250 lines by rejecting lines which clearly could not create any acceptable combination due to unavoidable intersection with neighboring tie lines; see Fig. S5A. The number of available combinations made from those 250 trial tie lines is about 5×10^{14} which is still too large to make the selection automatically. The trial tie lines which have minimal $\Delta \bar{s}$ do not form acceptable tie-line set since some of them intersect; see Fig. S5B. Therefore several trial tie lines with the

minimal $\Delta\bar{s}$ were taken as true tie lines for these points (shown as bold lines on Fig. S5B). For the rest of the points, the decision was made based on the selection criteria defined as the minimal sum of $\Delta\bar{s}$ and non-intersection with already available tie lines. Figure 5 in the main text shows the final 13 tie lines in the coexisting l_o - l_d region that were determined in this way.

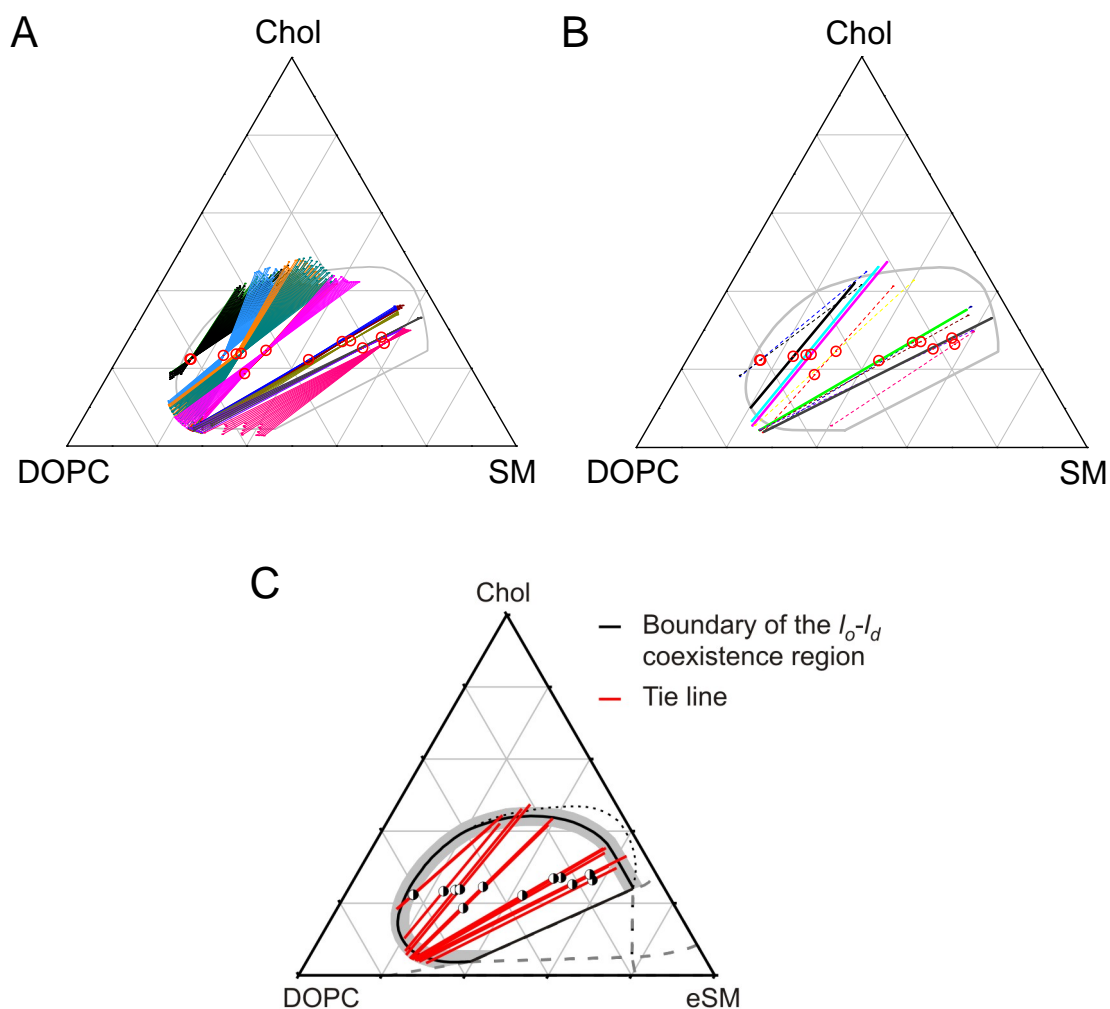


FIGURE S5 Tie lines in the l_o - l_d coexistence region. (A) All trial tie lines found for the composition points of the 13 fused vesicles (indicated with red open circles). The tie lines were selected under the condition that they do not cross the end tie line and that $\Delta\bar{s} < 2\%$, see text for details. The allowed deviation from the established coexistence curve was set to 2 mol% and 4.5 mol% from the binodals facing the single-phase l_d and l_o regions, respectively. (B) Trial tie-lines, one for each composition point, which have minimal $\Delta\bar{s}$, see text for details. (C) Final tie lines as in Fig. 5 in the main text.

Table S2 Coordinates of the found tie lines in the l_o - l_d coexistence region. The first column shows the composition of the vesicle used to determine the corresponding tie line. The last two columns show the angle between the tie line and the DOPC-eSM axis of the phase diagram and apparent free energies of lipid molecule transfer from the l_d to l_o phase.

Vesicle composition (DOPC/eSM/Chol)	Composition of the l_d phase			Composition of the l_o phase			Inclination angle of the tie line, °	Free energy of transfer, $k_B T$		
	DOPC	SM	Chol	DOPC	SM	Chol		ΔG^{DOPC}	ΔG^{SM}	ΔG^{Chol}
16:58:26	67.7	28.9	3.4	8.7	61.6	29.7	26.5	1.7	-1.1	-2.5
22:53:25	69.1	27.1	3.8	10.3	59.4	30.3	26.7	1.4	-1.3	-2.6
16:56:28	69.6	26.3	4.1	4.6	62.3	33.1	26.5	2.4	-1.1	-2.3
23:50:27	69.9	25.9	4.2	9.4	56.7	33.9	29.5	1.8	-1	-2.3
25:48:27	64.5	28.4	7.1	8.5	56.2	35.3	30.2	1.7	-1	-1.9
35:43:22	70.4	25.1	4.5	9.2	55.6	35.2	30.2	1.7	-1.1	-2.4
51:30:19	70.7	24.8	4.5	19.1	39.2	41.7	44.4	0.9	-0.8	-2.6
43:32:25	71.0	24.3	4.7	17.1	39.4	43.5	44.4	1	-0.9	-2.6
49:27:24	71.4	23.0	5.6	20.6	31.9	47.5	50.6	0.5	-1.1	-2.9
50:26:24	71.0	22.3	6.7	23.2	30.6	46.2	50.7	0.4	-1	-2.6
54:23:23	69.5	20.3	10.2	30.5	27.4	42.1	50.2	0.1	-1	-2.1
62:16:22	67.3	14.4	18.3	28.8	26.8	44.4	41.5	0.2	-1.2	-1.5
62:16:22	66.9	14.6	18.5	33.2	25.5	41.3	41.5	0	-1.3	-1.5

7. Creating multidomain vesicles

Consecutive electrofusion events allow us to create multidomain vesicles as shown in Fig. S6.

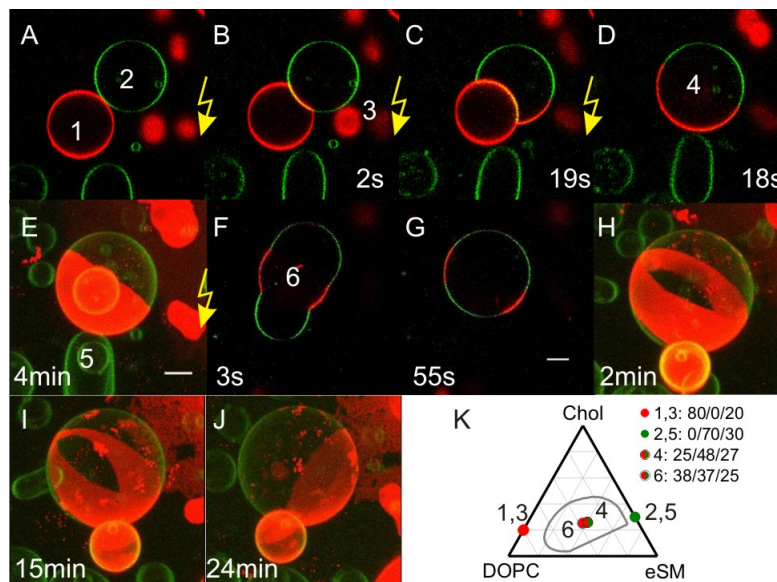


FIGURE S6 Formation of a three-domain vesicle by consecutive electrofusion of four vesicles (indicated with 1, 2, 3 and 5 in the images) with different compositions at 23°C. (A-D, F, G) Images acquired with confocal microscopy scans nearly at the equatorial plane of the fusing vesicles. (E, H-J) Three-dimensional projections. The sequence of pulses applied to the vesicles indicated with lightning symbol had the following amplitudes: 500kV/m, 300kV/m, 300kV/m, and 500kV/m. All pulses were 300 μ s long. The time stamps indicate the time after each pulse. The scale bars correspond to 10 μ m. (K) Phase diagram with the compositions of the six vesicles labeled from 1 to 6 in the confocal images.

References

1. Hell, S., and E. H. K. Stelzer. 1995. Lens aberrations in confocal fluorescence microscopy. In Handbook of biological confocal microscopy. J. B. Pawley, editor. Plenum Press, New York. 347-354.
2. Maulik, P. R., P. K. Sripada, and G. G. Shipley. 1991. Structure and Thermotropic Properties of Hydrated N-Stearoyl Sphingomyelin Bilayer-Membranes. *Biochim. Biophys. Acta* 1062:211-219.
3. Khelashvili, G. A., and H. L. Scott. 2004. Combined Monte Carlo and molecular dynamics simulation of hydrated 18:0 sphingomyelin-cholesterol lipid bilayers. *J. Chem. Phys.* 120:9841-9847.

4. Hofsäss, C., E. Lindahl, and O. Edholm. 2003. Molecular dynamics simulations of phospholipid bilayers with cholesterol. *Biophys. J.* 84:2192-2206.
5. Mathai, J. C., S. Tristram-Nagle, J. F. Nagle, and M. L. Zeidel. 2008. Structural determinants of water permeability through the lipid membrane. *J. Gen. Physiol.* 131:69-76.
6. Pan, J., S. Tristram-Nagle, N. Kucerka, and J. F. Nagle. 2008. Temperature dependence of structure, bending rigidity, and bilayer interactions of dioleoylphosphatidylcholine bilayers. *Biophys. J.* 94:117-124.
7. Smaby, J. M., M. M. Momsen, H. L. Brockman, and R. E. Brown. 1997. Phosphatidylcholine acyl unsaturation modulates the decrease in interfacial elasticity induced by cholesterol. *Biophys. J.* 73:1492-1505.